

Advantages and limitations of channel multiplexing for discrete-variable quantum key distribution

Indranil Maiti^{*1} and Mikołaj Lasota¹

¹Faculty of Physics, Astronomy and Informatics, Nicolaus Copernicus University, Grudziadzka 5, 87-100 Toruń, Poland

December 23, 2024

Abstract

Typically practical realizations of discrete-variable quantum key distribution (QKD) protocols, based on exchanging single-photon signals between the trusted parties, can provide its users with only very low key generation rates. One of the potential solutions for this problem, that can be adapted for the case of entanglement-based QKD schemes using broadband photon-pair sources, is to utilize wavelength-division-multiplexing (WDM) modules in order to split the photons with different wavelengths to separate detection channels and generate multiple keys in parallel. Here, we theoretically investigate this idea in the case of pulsed laser used to pump spontaneous parametric down-conversion source. We optimize the effective phase-matching function width of the nonlinear crystal, and the intensity and duration of the pump laser pulses in order to maximize the advantage of the overall key generation rate provided by the WDM-based QKD scheme over the traditional no-WDM scenario. The results of our analysis show that the considered method can significantly accelerate the production of cryptographic keys, but proper optimization of the photon-pair source is needed to exploit its full potential.

1 Introduction

Quantum key distribution (QKD) is a method to generate cryptographic keys between distant trusted parties [1]. Contrary to the classical protocols, the security of which relies on uncertain assumptions on the computational power accessible to a potential eavesdropper, the security of QKD schemes is based on fundamental laws of nature. Unfortunately, numerous imperfections of realistic setup elements required for the implementation of QKD protocols impose strong limitation on their performance, both in terms of maximal security distance and the obtainable key generation rate [2]. The latter can be particularly low in the case of discrete-variable (DV) protocols, that require using single photons or their approximations in the form of weak coherent pulses as information carriers. On the other hand DV QKD schemes are capable of distributing secret keys on several hundreds of kilometers [3, 4]. It is considerably longer than in the case of their continuous-variable counterparts [5], which are more vulnerable to photon loss, particularly in the case of entanglement-based setup configuration [6].

^{*}Corresponding author: indra@doktorant.umk.pl

Among the sources of photon pairs, required for the implementation of entanglement-based versions of DV QKD protocols, the most popular are the devices based on the spontaneous parametric down-conversion (SPDC) process [7, 8]. Their advantages include high generation and collection efficiency [9, 10, 11], high quality of the emitted photons [12, 13], good performance in room temperature, high versatility in terms of properties of the produced photons and relatively low construction cost. On the other hand, this type of source is probabilistic, meaning that the number of photon pairs generated from a single pump pulse follows some statistics, which is thermal in the case of single-mode SPDC process and gradually changes toward Poissonian when the number of contributing modes grow [14, 15]. Multipair emission events have negative influence on the QKD security, as has the effect of temporal broadening of SPDC photons, taking place during their propagation in dispersive media due to their relatively broad spectrum [16, 17].

However, the aforementioned disadvantages of SPDC sources can be turned into an actual advantage. To achieve this, both legitimate parties have to divide the spectrum of the received photons into several ranges and direct the photons from different ranges into separate detection systems. If the spectral correlation between the photons belonging to the same SPDC pair is relatively strong it can be possible to define multiple pairs of correlated systems to which these photons could go with very high probability (in other words the probability for a pair of photons to enter a pair of systems not defined as correlated is very small). Then, basing on coincident detection events observed in the correlated pairs of detectors, many cryptographic keys can be produced in parallel. If they are combined together at the end, the resulting overall key generation rate can become significantly higher than the rate obtainable from the traditional setup configuration.

This idea has been recently suggested by Pseiner et al. [18], who experimentally investigated the possibility to increase the achievable key generation rate in QKD system based on SPDC source pumped with continuous-wave (CW) laser. The authors of Ref. [18] utilized wavelength-division-multiplexing (WDM) modules to direct SPDC photons into separate detection setups. Such devices are one of the standard elements of modern classical communication systems [19]. In the context of QKD they have been studied in several papers exploring the possibility to perform simultaneous quantum and classical communication with the use of single fiber link [20, 21, 22] and quantum-classical communication networks [23, 24, 25].

In this work we adapt the idea introduced in Ref. [18] to theoretically research the possibility for increasing the key generation rate produced from the entanglement-based version of the BB84 protocol [26], realized with pulsed-pump SPDC source, when using WDM modules. In order to properly assess the potential advantage of this method we numerically optimize the parameters of the SPDC source, including the effective-phase matching function (EPMF) width of the nonlinear crystal, and the duration and intensity of the pump laser pulses, for various numbers of WDM channel pairs utilized by the trusted parties for QKD. We compare the results with the maximal key generation rate that can be obtained in traditional setup configuration, without WDM modules. We consider different properties of the WDM channels, including their width, separation and transmission profile. We analyze both the cases of SPDC source producing strongly negative and strongly positive spectral correlation between the pairs of generated photons. The presented results show that the overall key rate can indeed be significantly increased using the investigated method, but the achievable advantage strongly depends on the properties of the utilized SPDC source.

The paper is organized as follows. In Sec.2 we specify the considered setup configuration and discuss our assumptions on its main properties. The QKD security analysis is provided in Sec.3. Next, in Sec.4, we present the results of numerical simulations, done with the use of security formulas derived in Sec.3. Finally, in Sec.5 we summarize the main conclusions stemming from our investigation and discuss its planned continuation.

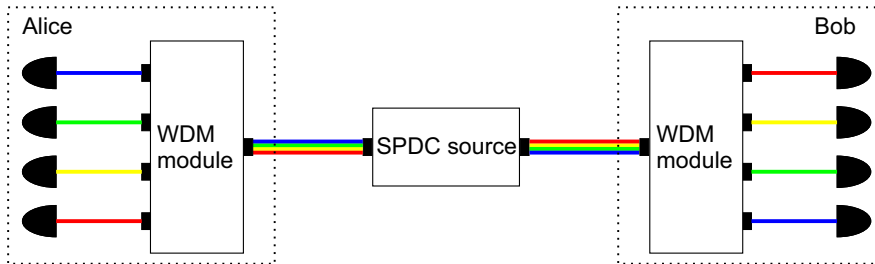


Figure 1: Schematic diagram of the considered setup.

2 Setup and assumptions

In this work we consider entanglement-based version of the BB84 protocol, with information encoded in photon polarization. A schematic diagram of the setup is presented in Fig.1. We assume that the pulsed-pump type II SPDC source, located in-between Alice and Bob, produces two-photon polarization states $|\psi^-\rangle = (|HV\rangle - |VH\rangle)/\sqrt{2}$. The spectral biphoton wavefunction can be conveniently approximated by [27, 28]:

$$f(\omega_s, \omega_i) \approx \sqrt{\frac{\tau_p}{\pi\sigma_{cr}}} \times \exp\left[-\frac{(\omega_s - \omega_i)^2}{\sigma_{cr}^2} - \frac{(\omega_s + \omega_i)^2\tau_p^2}{4}\right], \quad (1)$$

where ω_s and ω_i denote the angular frequency detunings of signal and idler photon, respectively, from their central values, τ_p is the pump laser pulse duration, and σ_{cr} is the EPMF width, characterizing the nonlinear crystal in which the SPDC process takes place. The parameters τ_p and σ_{cr} are convenient from experimental point of view, since they can be changed independently from each other, by modifying the pump laser and non-linear crystal utilized by the source, respectively. However, in some situations it is beneficial to use the quantities describing the properties of the generated pairs of photons, namely their spectral bandwidth, σ , and the spectral correlation coefficient, ρ . The relationship between the two sets of parameters mentioned above is as follows [29]:

$$\sigma = \frac{\sqrt{4 + \sigma_{cr}^2\tau_p^2}}{2\sqrt{2}\tau_p}, \quad (2)$$

$$\rho = \frac{4 - \sigma_{cr}^2\tau_p^2}{4 + \sigma_{cr}^2\tau_p^2}. \quad (3)$$

Without losing generality of the presented consideration we assume that the signal (idler) photons are always sent to Alice (Bob). At their arrival to the trusted parties' laboratories they pass through WDM modules, which direct them to different output channels, depending on their wavelengths. Finally, their polarizations are measured at the exit of the output channels. If the spectral correlation between the SPDC photons is relatively strong, $|\rho| \approx 1$, detecting one of them in a particular output channel by Alice allows her to predict with high probability the output channel of Bob's setup to which the corresponding photon from the same pair would go. This is illustrated in Fig.2, where we sketch the spectral wavefunction describing photon pairs generated by an SPDC source for the so-called negative spectral correlation scenario ($\rho < 0$) – panel (a) – and the positive spectral correlation scenario ($\rho > 0$) – panel (b). For both these cases an example of a set of correlated WDM channels that the trusted parties can use is also shown.

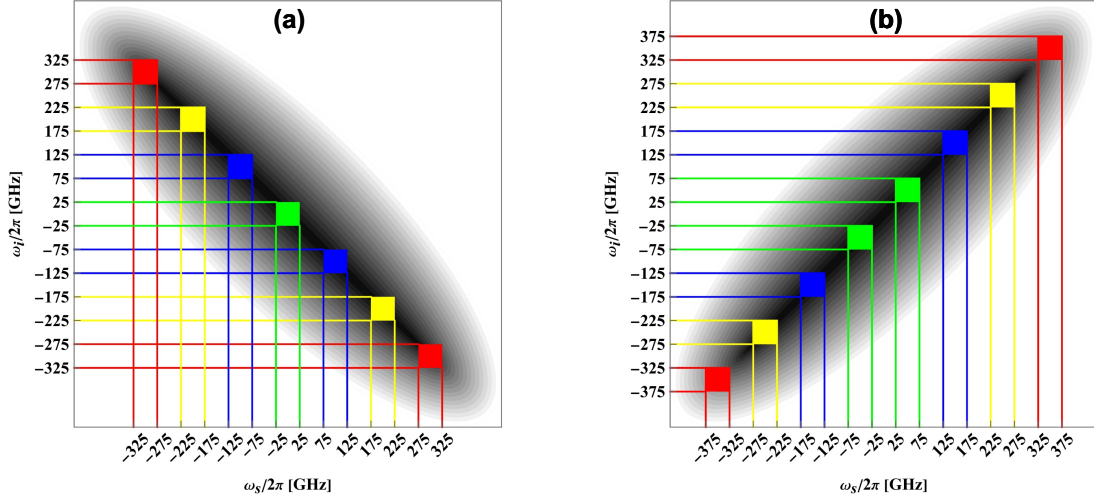


Figure 2: Examples of the spectral wavefunction for pairs of photons produced by the SPDC source in the case of (a) negative, (b) positive spectral correlation generated between them. The multicoloured squares indicate a grid of (a) seven or (b) eight WDM channel pairs, with rectangular transmission profiles, that can be used for separate key generation processes.

It is assumed that only if coincident clicks are observed at the outputs of any of the chosen channel pairs, Alice and Bob accept such event for the key generation process. On the contrary, coincident clicks from any other combination of WDM channels is automatically discarded due to high probability that they are caused by uncorrelated photons.

Various WDM channel transmission profiles can be found in the literature, depending particularly on the type of optical filters utilized by the WDM module [30]. In our investigation we consider two approximations of such profile, given by the rectangular and Gaussian functions. In the case of rectangular profile we assume that the probability for transmitting a photon with angular frequency ω by a particular channel, centered at ω_0 and with $\Delta\omega$ width, is given by:

$$F_{\omega_0}^{\text{rect}}(\omega) = \begin{cases} 1; & \omega_0 - \Delta\omega/2 \leq \omega \leq \omega_0 + \Delta\omega/2 \\ 0; & \text{otherwise} \end{cases} . \quad (4)$$

On the other hand, for Gaussian-shaped profile, parametrized by the standard deviation σ_f , we have:

$$F_{\omega_0}^{\text{Gauss}}(\omega) = \frac{1}{\sigma_f \sqrt{2\pi}} \times \exp \left[-\frac{(\omega - \omega_0)^2}{2\sigma_f^2} \right]. \quad (5)$$

We also assume that the separation between the neighboring WDM channels in terms of angular frequency is fixed to $\omega_{\text{sep}} = 2\pi \times 100$ GHz, which is typical value for a standard WDM channel grid. The slopes of realistic WDM channel transmission functions are typically much steeper than the Gaussian function, but not exactly vertical as in the rectangular one. Thus, the presented results of key generation rate calculation can be seen as the lower and upper bound, respectively, for the values that can be obtained when using practical WDM modules,

In order to properly describe the sets of channel pairs considered in our analysis let us introduce the channel pair identification number n and the total number of WDM channel pairs utilized by the trusted parties, N . We assume that if the spectral correlation generated between

the photon pairs produced by the SPDC source is negative, as in Fig.2 (a), then the central angular frequency detunings of the considered channel pairs are given by the set

$$\left\{ \omega_{s0}^{(n,-)}, \omega_{i0}^{(n,-)} \right\} = \left\{ -\frac{n}{2}\omega_{\text{sep}}, \frac{n}{2}\omega_{\text{sep}} \right\}. \quad (6)$$

If N is odd, Alice and Bob utilize the channel pairs with even identification numbers ranging from $-(N-1)$ to $N-1$. On the contrary, if N is even the channel pairs with odd identification numbers between $-N$ and N are used. For example the channel pairs illustrated in Fig. 2 (a) have the following identification numbers according to our notation: -6, -4, -2, 0, 2, 4, 6 (counting from left top red to right bottom red square). With such channel numbering system we fix the center of the WDM channel grid to coincide with the center of the biphoton wavefunction, regardless of how many channel pairs are utilized by the trusted parties. This choice is reasonable since it maximizes the obtainable overall key generation rate for any fixed value of N . It can be also seen that the individual key generation rates provided by the channel pairs with numbers $-n$ and n (represented by the squares of the same colors in Fig. 2) are equal to each other. Similar channel numbering system is used for the case of positive spectral correlation produced between the SPDC photons, but in this scenario the set of central angular frequency detunings considered in our analysis is modified to

$$\left\{ \omega_{s0}^{(n,+)}, \omega_{i0}^{(n,+)} \right\} = \left\{ \frac{n}{2}\omega_{\text{sep}}, \frac{n}{2}\omega_{\text{sep}} \right\}. \quad (7)$$

In the example of Fig. 2 (b), where eight channel pairs are pictured, their central angular frequency detunings are given by Eq. (7), with n taking the values from the following set: $\{-7, -5, -3, -1, 1, 3, 5, 7\}$.

Since the number of parameters describing the SPDC source and WDM modules, considered in this paper, is already quite high, we limit our analysis to the case of ideal photon-number-resolving detectors utilized by Alice and Bob, and lossy, but noiseless channels connecting them with the source. Therefore, the presented results are most relevant for medium-distance QKD implementations, where the probability for the signal emitted by the source to reach the measurement systems of the trusted parties is much larger than the overall probability to register noise, while the probability for Alice and/or Bob to observe more than one photon in a single WDM channel is negligible. We use the symbols T_A and T_B to denote the channels' transmittance. While the theoretical analysis is performed for the general case, in numerical simulations we focus solely on the symmetric situation, in which $T_A = T_B \equiv T$. The extension of this analysis to the more practical cases of noisy QKD setup and binary detectors is going to be presented in the follow-up to this paper, which is currently in preparation.

3 Key generation rate

The main quantity utilized for the security evaluation of QKD protocols is the key generation rate, defined as the number of secure key bits produced by the trusted parties per one use of the source. In general it can be expressed as [31]

$$K = p_{\text{sift}} p_{\text{acc}} [I(A : B) - \max(I_{EA}, I_{EB})], \quad (8)$$

where p_{sift} is the sifting probability, p_{acc} is the probability for Alice and Bob to accept the outcome of their measurements for the key generation process, $I(A : B)$ is the mutual information between the trusted parties and I_{EA} (I_{EB}) denotes the information gained by the eavesdropper on Alice's (Bob's) version of the raw key. For protocols with binary encoding, like BB84, $I(A :$

$B) = 1 - h(Q)$, where Q is the so-called quantum bit error rate (QBER) and $h(Q)$ denotes binary Shannon entropy. For the symmetric version of the BB84 protocol, considered here, $p_{\text{sift}} = 1/2$.

Let us now focus on one pair of correlated WDM channels utilized by Alice and Bob, centered at ω_{s0} and ω_{i0} , respectively. If the trusted parties employ ideal PNR detectors for their measurements, they can immediately uncover large-pulse attacks [32], that could potentially be performed by Eve. Therefore, they can automatically remove all the double click events from the key generation process and accept only the events when both of them received exactly one click in one of their detectors. If we denote by $p(i_H, i_V; j_H, j_V)$ the joint probability for Alice to measure i_H and i_V photons in her detectors for H - and V -polarized light, and for Bob to measure j_H and j_V photons in his detectors for H - and V - polarized light, respectively, then in this case

$$p_{\text{acc}} = p(1, 0; 1, 0) + p(1, 0; 0, 1) + p(0, 1; 1, 0) + p(0, 1; 0, 1). \quad (9)$$

Furthermore, since the pairs of photons produced by the source are supposed to be anti-correlated in polarization, the QBER can be calculated as

$$Q = \frac{p(1, 0; 1, 0) + p(0, 1; 0, 1)}{p_{\text{acc}}^{\text{PNR}}}. \quad (10)$$

In the entanglement-based version of the BB84 protocol photons belonging to different SPDC pairs are uncorrelated. Therefore, Eve cannot gain any information on the polarization state of the photon detected by either Alice or Bob by performing photon-number-splitting (PNS) attacks [2]. In this case the upper bound for the information on the raw key gained by her from general attacks on the BB84 protocol reads [33, 34]

$$I_{EA} = I_{EB} = h(Q). \quad (11)$$

Calculating the key generation rate requires expressing the probabilities $p(i_H, i_V; j_H, j_V)$ in terms of the setup parameters. To this end let us first denote the probability for both photons belonging to a single SPDC pair to enter the two considered WDM channels by p_{++} . If the channels have rectangular transmission profile, given by Eq. (4), then

$$p_{++}^{\text{rect}} = \int_{\omega_{s0}-\Delta\omega/2}^{\omega_{s0}+\Delta\omega/2} d\omega_s \int_{\omega_{i0}-\Delta\omega/2}^{\omega_{i0}+\Delta\omega/2} d\omega_i |f(\omega_s, \omega_i)|^2, \quad (12)$$

where the spectral biphoton wavefunction is given by the formula (1). In the case of Gaussian transmission profile (5) the aforementioned probability transforms into

$$p_{++}^{\text{Gaus}} = \int_{-\infty}^{+\infty} d\omega_s \int_{-\infty}^{+\infty} d\omega_i |f(\omega_s, \omega_i)|^2 \times \exp \left[-\frac{(\omega_s - \omega_{s0})^2 + (\omega_i - \omega_{i0})^2}{\sigma_f^2} \right]. \quad (13)$$

Analogously we define the probabilities that only Alice's photon enters her WDM channel, only Bob's photon enters his WDM channel and none of the photons enter the two channels by p_{+-} , p_{-+} and p_{--} , respectively. They read:

$$p_{+-}^{\text{rect}} = \int_{\omega_{s0}-\Delta\omega/2}^{\omega_{s0}+\Delta\omega/2} d\omega_s \int_{-\infty}^{+\infty} d\omega_i |f(\omega_s, \omega_i)|^2 - p_{++}^{\text{rect}}, \quad (14)$$

$$p_{-+}^{\text{rect}} = \int_{-\infty}^{+\infty} d\omega_s \int_{\omega_{i0}-\Delta\omega/2}^{\omega_{i0}+\Delta\omega/2} d\omega_i |f(\omega_s, \omega_i)|^2 - p_{++}^{\text{rect}}, \quad (15)$$

$$p_{--}^{\text{rect}} = 1 - p_{+-}^{\text{rect}} - p_{-+}^{\text{rect}} + p_{++}^{\text{rect}}, \quad (16)$$

$$p_{+-}^{\text{Gaus}} = \int_{-\infty}^{+\infty} d\omega_s \int_{-\infty}^{+\infty} d\omega_i |f(\omega_s, \omega_i)|^2 \times \exp \left[-\frac{(\omega_s - \omega_{s0})^2}{\sigma_f^2} \right] - p_{+++}^{\text{Gaus}}, \quad (17)$$

$$p_{-+}^{\text{Gaus}} = \int_{-\infty}^{+\infty} d\omega_s \int_{-\infty}^{+\infty} d\omega_i |f(\omega_s, \omega_i)|^2 \times \exp \left[-\frac{(\omega_i - \omega_{i0})^2}{\sigma_f^2} \right] - p_{+++}^{\text{Gaus}} \quad (18)$$

and

$$p_{--}^{\text{Gaus}} = 1 - p_{+-}^{\text{Gaus}} - p_{-+}^{\text{Gaus}} + p_{+++}^{\text{Gaus}}. \quad (19)$$

If we denote the probability for the SPDC source to produce k pairs of X -polarized signal photons and Y -polarized idler photons in an individual photon generation event by $\pi_{XY}(k)$, then the joint probability for m_H H-polarized photons and m_V V-polarized photons to enter Alice's WDM channel and n_H H-polarized photons and n_V V-polarized photons to enter Bob's WDM channel is equal to

$$\begin{aligned} q(m_H, m_V, n_H, n_V) &= \sum_{\alpha=0}^{\min[m_H, n_V]} \sum_{\beta=0}^{\min[m_V, n_H]} \sum_{\gamma=0}^{\infty} \sum_{\delta=0}^{\infty} \pi_{HV}(m_H + n_V + \gamma - \alpha) \\ &\times \pi_{VH}(m_V + n_H + \delta - \beta) p_{++}^{\alpha+\beta} p_{+-}^{m_H+m_V-\alpha-\beta} p_{-+}^{n_H+n_V-\alpha-\beta} p_{--}^{\gamma+\delta} \binom{m_H + n_V + \gamma - \alpha}{\alpha} \\ &\times \binom{m_H + n_V + \gamma - 2\alpha}{\gamma} \binom{m_H + n_V - 2\alpha}{m_H - \alpha} \binom{m_V + n_H - 2\beta}{m_V - \beta} \binom{m_V + n_H + \delta - 2\beta}{\delta} \\ &\times \binom{m_V + n_H + \delta - \beta}{\beta}. \end{aligned} \quad (20)$$

Finally, the probability $p(i_H, i_V, j_H, j_V)$ can be calculated as

$$\begin{aligned} p(i_H, i_V, j_H, j_V) &= \sum_{m_H=i_H}^{\infty} \sum_{m_V=i_V}^{\infty} \sum_{n_H=j_H}^{\infty} \sum_{n_V=j_V}^{\infty} q(m_H, m_V, n_H, n_V) T_A^{i_H+i_V} \\ &\times (1 - T_A)^{m_H+m_V-i_H-i_V} T_B^{j_H+j_V} (1 - T_B)^{n_H+n_V-j_H-j_V}. \end{aligned} \quad (21)$$

By inserting the relevant formulas for p_{acc} and Q , derived above, with $p(i_H, i_V, j_H, j_V)$ given by Eq. (21), into Eq. (8) one can estimate lower bound on the key generation rate produced from a pair of WDM channels, centered at the angular frequency detunings $\{\omega_{s0}, \omega_{i0}\}$. The overall key rate, generated from all of the channel pairs utilized by Alice and Bob, can be calculated as the sum of individual key rates obtained for the set of angular frequencies provided by Eq. (6) or Eq. (7), depending on the type of spectral correlation generated between the SPDC photons. In the next section we present the results of such calculations.

4 Numerical simulation

4.1 Key generation without WDM modules

Before focusing on the setup configuration presented in Fig. 1 let us estimate the key generation rate that can be obtained by the trusted parties when utilizing the traditional scheme, without WDM modules. In this case the formula (21) simplifies to

$$\begin{aligned} p_{\text{noWDM}}(i_H, i_V, j_H, j_V) &= \sum_{m=\max\{i_H, j_V\}}^{\infty} \sum_{n=\max\{i_V, j_H\}}^{\infty} q_{\text{noWDM}}(m, n) T_A^{i_H+i_V} \\ &\times (1 - T_A)^{m+n-i_H-i_V} T_B^{j_H+j_V} (1 - T_B)^{m+n-j_H-j_V}, \end{aligned} \quad (22)$$

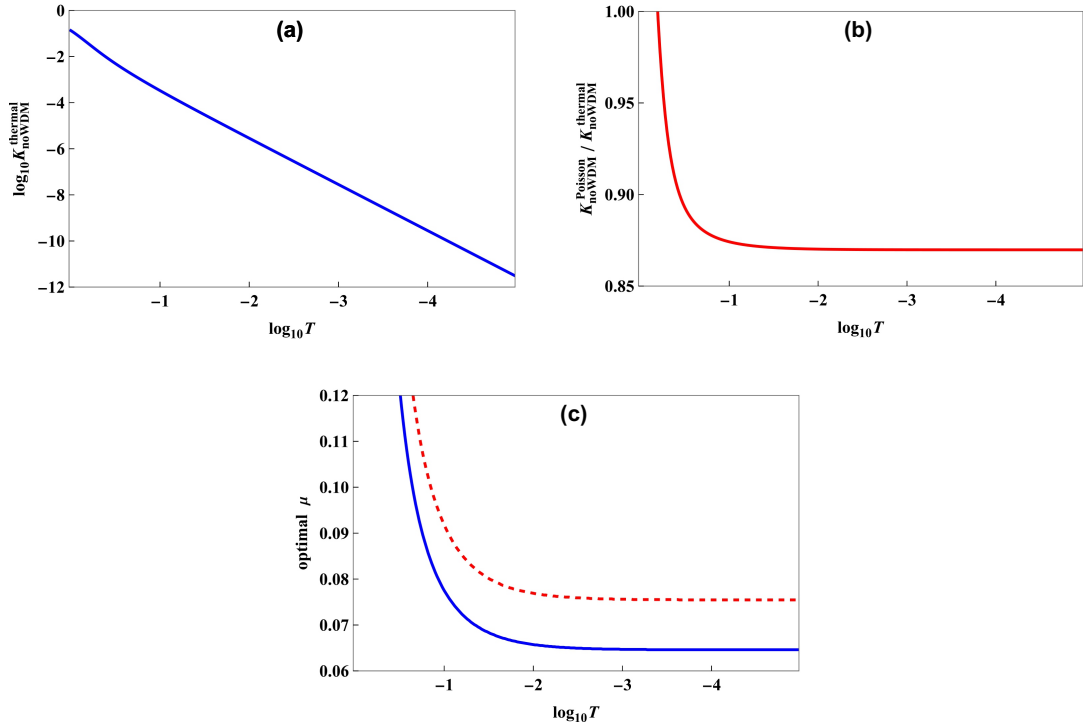


Figure 3: (a) Lower bound for the key generation rate that can be obtained by Alice and Bob with the use of the SPDC source producing spectrally uncorrelated photons, $\rho = 0$, in traditional QKD setup without WDM modules, plotted as a function of the transmittance of the symmetric channels connecting the source with the trusted parties, T . (b) The ratio between the key generation rate that can be obtained by Alice and Bob with the use of the SPDC source producing photons with strong spectral correlation, $|\rho| \approx 1$, in traditional QKD setup without WDM modules, and the key generation rate illustrated in panel (a). The calculated key generation rates are optimized over the mean number of photons produced by the SPDC source in a single polarization mode per one attempt, μ . (c) The optimal values of μ for the cases of spectrally uncorrelated (blue solid line) and strongly correlated (red dashed line) photons.

where

$$q_{\text{noWDM}}(m, n) = \pi_{HV}(m) \pi_{VH}(n) \quad (23)$$

is the joint probability for the source to produce m pairs of H -polarized signal and V -polarized idler photons and n pairs of V -polarized signal and H -polarized idler photons from a single pump pulse.

The key generation rate depends on the statistics of photon pairs produced by the SPDC source. For single-spectral-mode SPDC process, which takes place when no spectral correlation between the signal and idler photons can be observed, *i.e.* $\rho = 0$, the number of photon pairs generated in each of the two polarization modes follows thermal probability distribution [35]. The lower bound for the key generation rate, denoted by $K_{\text{noWDM}}^{\text{thermal}}$, produced in this case, optimized over the power of the source, which is proportional to the parameter μ , calculated as a function of the transmittance of the channels connecting the source with the trusted parties, is presented in Fig. 3(a). The plot is only slightly deviated from the linear function, as could be expected

from the log-log type of key generation rate plot in the noiseless case. The deviation can be observed only for relatively high values of the channel transmittance and its origin stems from the non-negligible number of multi-click events that are registered in this scenario.

On the other hand, in the limit of very strong spectral correlation, $|\rho| \approx 1$, the number of contributing spectral modes approaches infinity and the photon pair statistics becomes Poissonian [35]. The comparison between the key generation rates that can be obtained by Alice and Bob in the Poissonian ($K_{\text{noWDM}}^{\text{Poisson}}$) and thermal ($K_{\text{noWDM}}^{\text{thermal}}$) cases is shown in Fig. 3 (b). Unless the transmittance of the channels is very high, the rate calculated for the thermal statistics of the emitted photon pairs is slightly higher. For $T \rightarrow 0$ the difference asymptotically approaches 13%. To understand the reason for such outcome let us consider the events when the source produces two photon pairs in total. In this case the error in the raw key is generated only if one HV pair and one VH pair were emitted, and the trusted parties detect photons from two different pairs. If two HV or two VH pairs were produced the error would not appear regardless of which photons are ultimately detected. In the thermal case the joint probability for one HV pair and one VH pair to be emitted is equal to $\mu^2/(\mu+1)^4$ and is the same as the probability for two HV or two VH pairs to be produced. On the other hand in the Poissonian case the probability for one HV pair and one VH pair to be emitted, equal to $\mu^2 e^{-2\mu}$, is two times larger than the generation probabilities for either two HV or two VH pairs. After performing similar analysis for the scenarios of more than two photon pairs being created by the SPDC source from a single pump pulse, one can arrive at the conclusion that for a given value of μ the higher QBER should be expected in the case when the number of photon pairs produced in a single polarization mode follows Poissonian statistics. Thus, the optimal value of μ for the thermal case turns out to be slightly higher than in the Poissonian case, as can be seen in Fig. 3 (c), leading to larger key generation rate.

4.2 Key generation with WDM modules – negative spectral correlation

Taking the results presented in Fig. 3 into account, it is reasonable to adopt $K_{\text{noWDM}}^{\text{thermal}}$ as the reference to which we compare the key generation rate obtained by the trusted parties when using WDM modules in their QKD setup, as pictured in Fig. 1. For this purpose let us define the gain function

$$G = K_{\text{WDM}}^{\text{total}} / K_{\text{noWDM}}^{\text{thermal}}, \quad (24)$$

where $K_{\text{WDM}}^{\text{total}}$ is the sum of all the key rates estimated with the use of the formulas presented in Sec. 3 for each pair of WDM channels utilized by Alice and Bob for the separate key generation process. All the calculations of $K_{\text{WDM}}^{\text{total}}$, the results of which are presented below, were performed with the assumption that the statistics of photon pairs emitted by the SPDC source can be approximated with the Poisson probability distribution. This simplification is reasonable when the spectral correlation between the signal and idler photons is relatively strong. While it changes the obtained key rates slightly, this effect is insignificant to the derived conclusions (see the Appendix for more detailed discussion).

We start the analysis from the scenario of the negative spectral correlation between the signal and idler photons produced by the SPDC source, in which case it is reasonable to establish the pairs of WDM channels according to the formula (6). In Fig. 4 (a) we present the dependence of the gain function on the pump laser pulse duration for various numbers of WDM channel pairs utilized to produce the key, calculated for $\sigma_{cr} = 3$ THz and optimized over the parameter μ . While the plots were made for $T = 10^{-3}$, the results are approximately independent from the transmittance of the channel as long as $T < 10^{-1}$. As shown in Fig. 4 (a), regardless of the number of WDM channel pairs utilized by Alice and Bob, the gain G grows with increasing pump laser pulse duration, reaching an asymptotic value for $\tau_p \rightarrow \infty$. When N is small, this value is

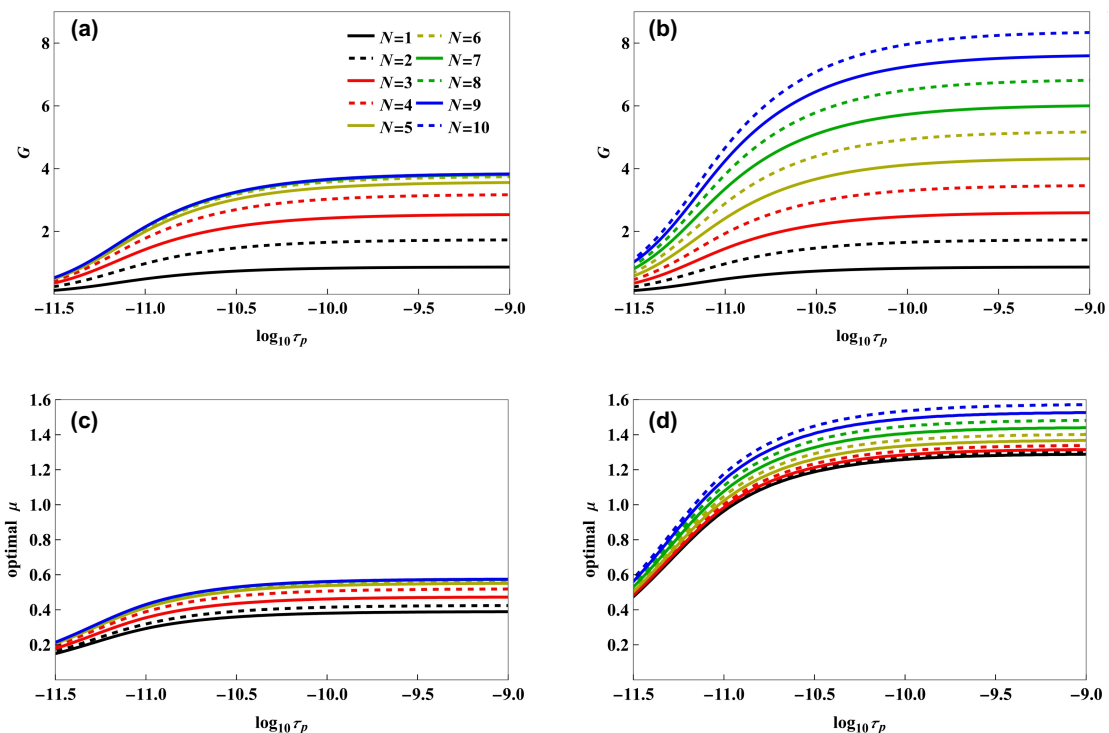


Figure 4: The gain function, defined with Eq. (24), plotted against the pump laser pulse duration, τ_p , for the EPMF width equal to (a) $\sigma_{cr} = 3$ THz and (b) $\sigma_{cr} = 10$ THz. The plots are maximized over the mean number of photon pairs emitted by the SPDC source in a single polarization mode μ and the optimal values of this parameter are shown in panels (c) and (d), respectively. Different colors and styles of all the lines correspond to various numbers of WDM channel pairs, N , utilized by Alice and Bob, as shown on the legend in panel (a). The transmission profiles of WDM channels is assumed to be rectangular and their central angular frequencies are defined according to Eq. (6). All the results are calculated for the transmittance of the channels connecting the source with the trusted parties equal to $T = 10^{-3}$.

equal to $NK_{\text{noWDM}}^{\text{Poisson}}/K_{\text{noWDM}}^{\text{thermal}}$. However, when $N > 6$ the G function stops increasing further with N . The reason for this behaviour is the assumed value of the EPMF width σ_{cr} , which is the primary parameter responsible for the width of the spectral biphoton wavefunction $f(\omega_s, \omega_i)$ in the diagonal direction on the $\{\omega_s, \omega_i\}$ grid. This can be seen by comparing the panels (a) and (b) in Fig. 5. As it turns out, for $\sigma_{cr} = 3$ THz the values assumed by $f(\omega_s, \omega_i)$ for channel pairs with numbers $n < -5$ or $n > 5$ are so small that there is no significant contribution to the overall key rate coming from them. Therefore, extending the number of WDM channel pairs utilized by the trusted parties to more than six does not improve $K_{\text{WDM}}^{\text{total}}$ anymore. In order to better the situation one has to increase σ_{cr} . This is confirmed in Fig. 4(b), where $\sigma_{cr} = 10$ THz and one can observe steady growth of the gain function with N at least up to $N = 10$.

Broader biphoton wavefunction in the diagonal direction means also that the probability for signal and idler photons to enter a given pair of WDM channels becomes smaller. Therefore, the optimal values of μ , maximizing the overall key generation rate, are significantly higher for $\sigma_{cr} = 10$ THz than for $\sigma_{cr} = 3$ THz. This can be confirmed by comparing the panels (c) and (d)

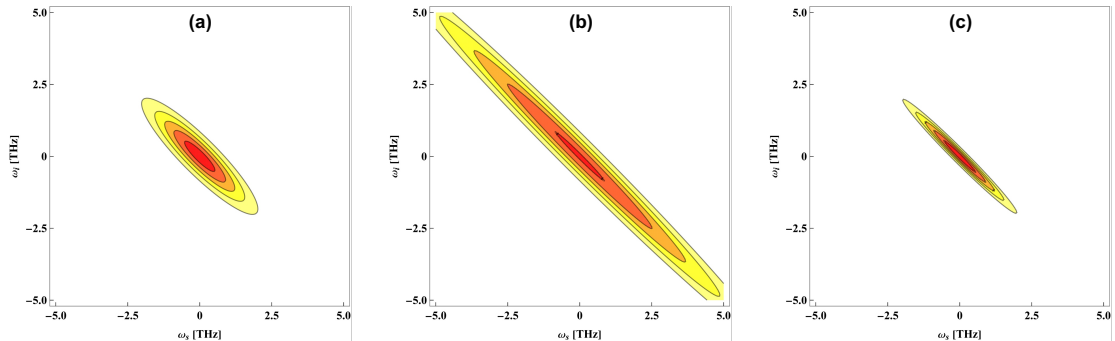


Figure 5: Spectral biphoton wavefunction $f(\omega_s, \omega_i)$, given by Eq. (1), plotted for (a) $\sigma_{cr} = 3\text{THz}$ and $\tau_p = 3\text{ps}$, (b) $\sigma_{cr} = 10\text{THz}$ and $\tau_p = 3\text{ps}$, (c) $\sigma_{cr} = 3\text{THz}$ and $\tau_p = 8\text{ps}$.

of Fig. 4. There, one can also observe an asymptotic growth of optimal μ with $\tau_p \rightarrow \infty$, regardless of the EPMF width or the number of WDM channel pairs utilized by Alice and Bob. This growth can be explained by the fact that pump laser pulse duration is the primary factor governing the width of the spectral biphoton wavefunction in the antidiagonal direction, as can be seen by comparing the panels (a) and (c) in Fig. 5. The longer τ_p is, the narrower $f(\omega_s, \omega_i)$ becomes, lowering the probabilities p_{+-} and p_{-+} , given by the formulas (14) and (15) respectively, that contribute to the QBER. Therefore, while the pump laser pulse duration does not influence the number of channel pairs from which Alice and Bob can get significant contribution to the overall key generation rate, its value becomes important for the key rate that can be obtained from every single pair.

From the above analysis it would appear that regardless of the EPMF width it is beneficial for the trusted parties to choose τ_p as long as possible. However, in practice it is more important to maximize the key rate that can be obtained per unit of time, R , than the key rate per one use of the source, given by the formula (8). The relationship between the two quantities is

$$R = f_r K, \quad (25)$$

where f_r is the repetition rate of the source. In realistic scenario f_r is primarily limited by the longest recovery time of the utilized setup elements τ_{rec} (*e.g.* the time needed by the source of photons to produce another signal or the dead time of the detectors), which is generally independent from the signal properties. However, if the pump pulses were very long, the main limitation on f_r would come from the requirement for proper separation between the subsequent signals emitted by the source. In Fig. 6 we plot the key generation rate per unit of time, optimized over μ , calculated as a function of the pump laser pulse duration for the case when $\sigma_{cr} = 10\text{THz}$. For the purpose of this calculation we assumed that reasonable separation between the pump laser pulses is equal to $3\tau_p$ and therefore

$$f_r = \min \{1/\tau_{\text{rec}}, 1/(3\tau_p)\}. \quad (26)$$

The plots were made for four different values of τ_{rec} . While the figure illustrates only the case of a single WDM channel pair utilized by Alice and Bob, the general behaviour of the calculated function is independent of N . The conclusion from Fig. 6 is that as long as $\tau_{\text{rec}} > 10\text{ps}$ (which would be extremely hard to break with the use of currently available technology) the optimal value of pump laser pulse duration, maximizing the key generation rate per unit of time, would be equal to $\tau_p^{\text{opt}} = \tau_{\text{rec}}/3$.

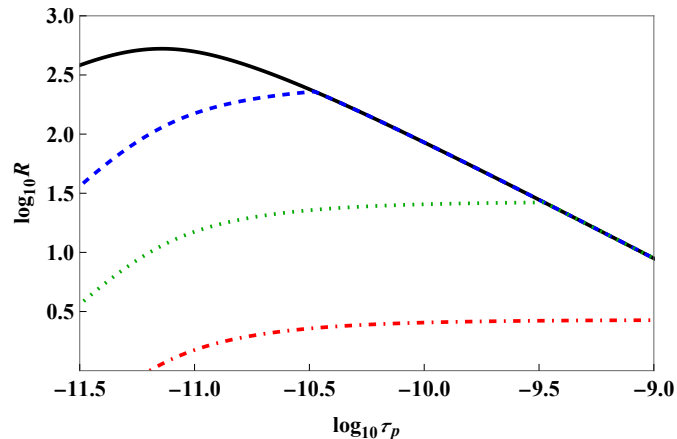


Figure 6: The lower bound for the number of bits of the secure key per unit of time, R , that can be obtained by Alice and Bob from the central WDM channels pair (*i.e.* the one with $n = 0$ in Eq. (6)) with rectangular transmission profile, plotted as a function of pump laser pulse duration, τ_p , with the assumption that the repetition rate of the source is given by the formula (26). The recovery time for the setup is assumed equal to $\tau_{\text{rec}} = 10$ ns (red, dot-dashed line), $\tau_{\text{rec}} = 1$ ns (green, dotted line), $\tau_{\text{rec}} = 100$ ps (blue, dashed line) and $\tau_{\text{rec}} = 0$ (black, solid line). The plots are made for the EPMF width $\sigma_{cr} = 10$ THz and the transmittance of the channels connecting the source with the trusted parties equal to $T = 10^{-3}$.

In realistic situation it is reasonable to expect the setup recovery time of the order of one nanosecond. Therefore, in Fig. 7 (a) we plot the gain function optimized over μ against the EPMF width with the assumption that $\tau_p^{\text{opt}} \approx 333$ ps. As already concluded from the comparison between the panels (a) and (b) of Fig. 4, the higher σ_{cr} becomes, the more WDM channel pairs can contribute to the overall key generation rate, which could potentially grow to infinity for $\sigma_{cr} \rightarrow \infty$. However, in practice this parameter of the SPDC source is always limited, depending on the type of utilized nonlinear material. For example in the case of bulk BBO crystal the values of σ_{cr} between 10^{11} Hz and 10^{13} Hz were shown to be realistically achievable [17]. Fig. 7 (a) can be also used to assess the number of WDM channel pairs that can be effectively employed to increase the key generation rate in situations when the SPDC source is already decided and the value of EPMF width is fixed.

The optimal mean number of photon pairs produced by the source in a single polarization mode, corresponding to the results presented in Fig. 7 (a), is illustrated in the panel (b) of the same figure. With $\sigma_{cr} \rightarrow \infty$ this quantity also grows to infinity. However, for even number of WDM channel pairs utilized by Alice and Bob one can observe $\mu \rightarrow \infty$ also when the value of σ_{cr} is very small. Similar behavior cannot be seen when N is odd. The reason for this difference stems from our assumption regarding the WDM channel positions, explained in details in Sec. 2. When $\sigma_{cr} < 1$ THz the spectral biphoton wavefunction $f(\omega_s, \omega_i)$ becomes so narrow in the diagonal direction that the probability for the SPDC photon pair to enter any pair of WDM channels beside the one with $n = 0$ is close to zero. However, this pair of channels is part of the WDM grid only in the odd N case. Therefore, when N is even the power of the pump laser has to be significantly higher to produce decent overall key rate.

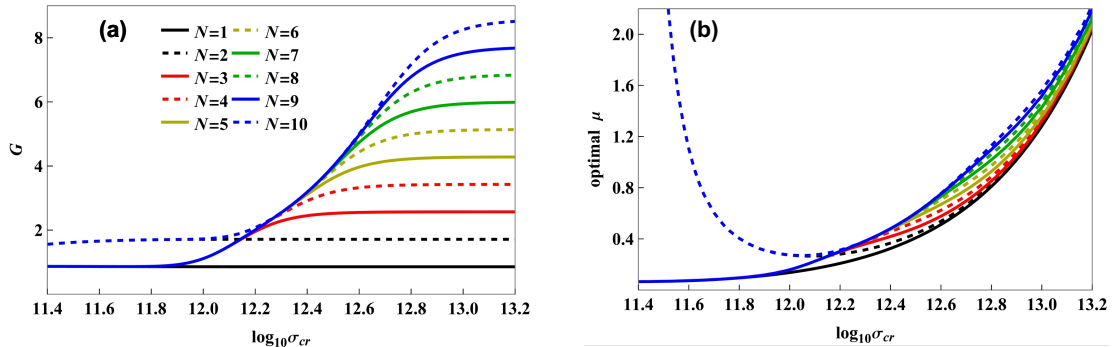


Figure 7: (a) The gain function, defined with Eq. (24), plotted against the EPMF width, σ_{cr} , for the pump laser pulse duration equal to $\tau_p = 333$ ns. The plots are maximized over the mean number of photon pairs emitted by the SPDC source in a single polarization mode, μ . Different colors and styles of the lines correspond to various numbers of WDM channel pairs, N , utilized by Alice and Bob, as shown on the legend. The transmission profiles of WDM channels is assumed to be rectangular and their center angular frequencies are defined according to Eq. (6). All the results are calculated for the transmittance of the channels connecting the source with the trusted parties equal to $T = 10^{-3}$. (b) The optimal values of μ , corresponding to the results illustrated in panel (a).

4.3 Key generation with WDM modules – positive spectral correlation

Utilizing WDM modules to increase $K_{\text{WDM}}^{\text{total}}$ is also possible when the SPDC source generates photons with strong positive spectral correlation. In this situation the corresponding WDM channel pairs should be defined according to the formula (7). As illustrated in Fig. 2 (b) they are placed on the anti-diagonal of the $\{\omega_s, \omega_i\}$ grid. Therefore, the effects of changing the values of the source parameters, σ_{cr} and τ_p , on the overall key rate are reversed in comparison to the case of negative spectral correlation, analyzed in Sec. 4.2.

When the positively correlated photons are produced, the modification of the pump laser pulse duration is responsible for adjusting the number of WDM channel pairs, from which the trusted parties can be able to obtain non-negligible contribution to the overall key. This effect is presented in Fig. 8 (a) where we plotted the gain G as a function of τ_p for $\sigma_{cr} = 10$ GHz and for up to ten WDM channel pairs used by Alice and Bob. The observed behavior resembles the $G(\sigma_{cr})$ dependence for the case of negative spectral correlation, shown previously in Fig. 7 (a). Also the corresponding plot of the optimal mean number of photon pairs generated in single polarization mode as a function of the pump laser pulse duration, illustrated in Fig. 8 (b), exhibits evident similarity to Fig. 7 (b). From Fig. 8 (a) one can conclude that the shorter the pump laser pulse duration is, the more WDM channel pairs can contribute to the QBER and it is theoretically possible to increase the overall key generation rate to arbitrary values when $\tau_p \rightarrow 0$. However, similarly as the realistic values of the EPMF width bound the achievable key rate in the case of negative spectral correlation, limited ability to produce ultrashort laser pulses does it in the positive-correlation scenario.

While in the case of positive spectral correlation the number of WDM channel pairs contributing to the overall key turns out to be almost independent of the EPMF width, σ_{cr} is the main parameter influencing the secret key rate that can be distilled from a single pair of channels. This relationship is investigated in Fig. 9 (a), where the function $G(\sigma_{cr})$ is plotted for the pump laser pulse duration $\tau_p = 100$ fs. When $\sigma_{cr} \rightarrow 0$ the gain approximately reaches the value of

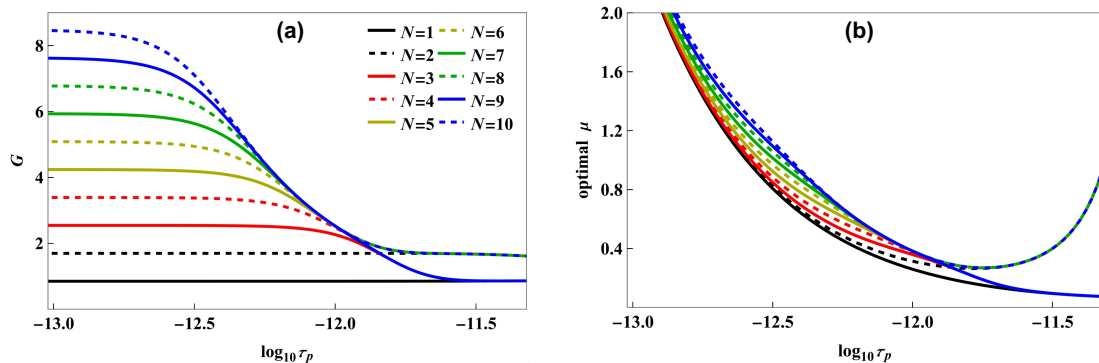


Figure 8: (a) The gain function, defined with Eq. (24), plotted against the pump laser pulse duration, τ_p , for the EPMF width equal to $\sigma_{cr} = 10$ GHz. Different colors and styles of all the lines correspond to various numbers of WDM channel pairs, N , utilized by Alice and Bob, as shown on the legend. The transmission profiles of WDM channels is assumed to be rectangular and their central angular frequencies are defined according to Eq. (7). The results are calculated for the transmittance of the channels connecting the source with the trusted parties equal to $T = 10^{-3}$. The plots are maximized over the mean number of photon pairs emitted by the SPDC source in a single polarization mode, μ . (b) Optimal values of μ corresponding to the results shown in panel (a).

$NK_{\text{noWDM}}^{\text{Poisson}}/K_{\text{noWDM}}^{\text{thermal}}$. On the other hand, for $\sigma_{cr} > 100$ GHz one can see evident decrease of the presented function.

4.4 Influence of WDM channels' properties on the overall key generation rate

All the plots shown in Secs. 4.2–4.3 were produced with a set of specific assumptions on the properties of individual channels provided by the WDM modules utilized by the trusted parties. In particular, we considered WDM channels with rectangular transmission profiles, given by Eq. (4), with the channel width $\Delta\omega = 2\pi \times 50$ GHz and the separation between the neighboring channels equal to $\omega_{\text{sep}} = 2\pi \times 100$ GHz. To make our analysis more general in this subsection we investigate how modifying the above assumptions can influence the results presented before.

Let us first focus on the channel width. In Fig. 10 (a) we compare the gain, G , plotted as a function of the EPMF width, calculated for two different values of $\Delta\omega$. The case of $\Delta\omega = 2\pi \times 100$ GHz can be treated as an ideal situation, in which the channels are completely separated from each other, although there is no gap between them. On the other hand WDM module with the channel width of $\Delta\omega = 2\pi \times 10$ GHz and separation of $\omega_{\text{sep}} = 2\pi \times 100$ GHz would be quite ineffective, as most of the signal and idler photons would be blocked by it. To make Fig. 10 (a) easier to read only the results for odd number of channel pairs utilized by Alice and Bob are shown. The outcomes for even N are completely analogous.

The difference between the values of G that can be obtained for $\Delta\omega = 2\pi \times 100$ GHz and $\Delta\omega = 2\pi \times 10$ GHz turns out to be relatively small, because larger loss of photons, observed in the latter case, can be neutralized by increasing the mean number of photons produced by the SPDC source in a single polarization mode per pulse. This can be clearly seen in Fig. 10 (b), where we plot the optimal μ corresponding to the results shown in panel (a). Still, the maximal value of the gain function turns out to be slightly higher for $\Delta\omega = 2\pi \times 100$ GHz. There are two reasons

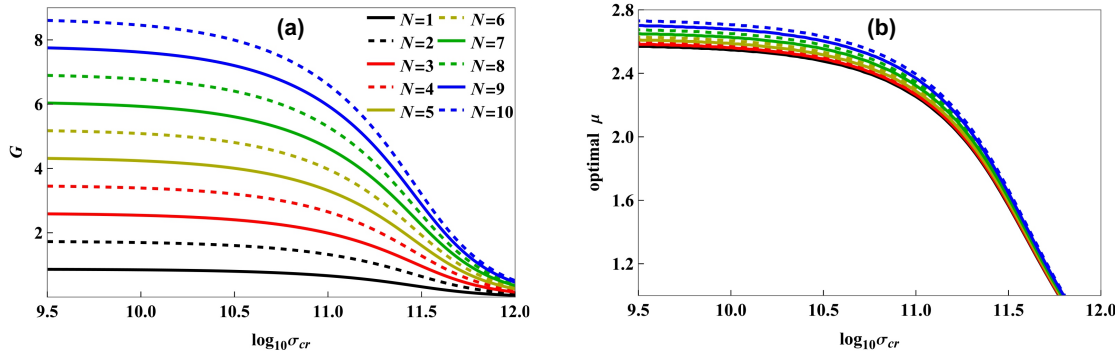


Figure 9: (a) The gain function, defined with Eq. (24), plotted against the EPMF width, σ_{cr} , for the pump laser pulse duration equal to $\tau_p = 100$ fs. The plots are maximized over the mean number of photon pairs emitted by the SPDC source in a single polarization mode, μ . Different colors and styles of the lines correspond to various numbers of WDM channel pairs, N , utilized by Alice and Bob, as shown on the legend. The transmission profiles of WDM channels is assumed to be rectangular and their center angular frequencies are defined according to Eq. (7). All the results are calculated for the transmittance of the channels connecting the source with the trusted parties equal to $T = 10^{-3}$. (b) The optimal values of μ , corresponding to the results illustrated in panel (a).

for this outcome. Firstly, the relative difference between the values of the probabilities p_{++}^{rect} , calculated for individual channel pairs, grow when the channels become narrower. This means that the values of μ , optimizing the key rate provided by each of these pairs, are more imbalanced, which negatively affects the optimization capability of the overall system. Furthermore, when the channels are narrower, the relative width of the spectral biphoton wavefunction for a given value of τ_p increases. It negatively affects the QBER and slightly decreases the key generation rate obtainable from each individual WDM channel pair.

While the previously assumed separation between the neighboring WDM channels is standard for classical communication networks, WDM modules with other values of ω_{sep} can be also utilized. Therefore, it is useful to investigate how the overall key generation rate provided by the QKD system with N WDM channel pairs would change if the channel separation is modified from ω_{sep} to $A\omega_{\text{sep}}$, where A is an arbitrary positive number. This task can be easily resolved by realizing that the probabilities p_{++}^{rect} , p_{+-}^{rect} , p_{-+}^{rect} and p_{--}^{rect} are invariant under the following transformation of the relevant variables:

$$\begin{cases} \omega_{\text{sep}} & \rightarrow & A\omega_{\text{sep}} \\ \Delta\omega & \rightarrow & A\Delta\omega \\ \sigma_{cr} & \rightarrow & A\sigma_{cr} \\ \tau_p & \rightarrow & \tau_p/A \end{cases} \quad (27)$$

Thus, the overall key generation rate for the case of WDM channel separation equal to $A\omega_{\text{sep}}$ can be found by considering the standard value of $\omega_{\text{sep}} = 2\pi \times 100$ GHz with channel width and SPDC source properly adjusted, according to Eq. (27).

The comparison between the gain function values calculated for the cases of rectangular and Gaussian profiles of the WDM channel transmission is presented in Fig. 11 (a). While the key generation rate that can be obtained just from the central WDM channel pair ($N = 1$) is approximately independent on the EPMF width in the rectangular case, the situation is different

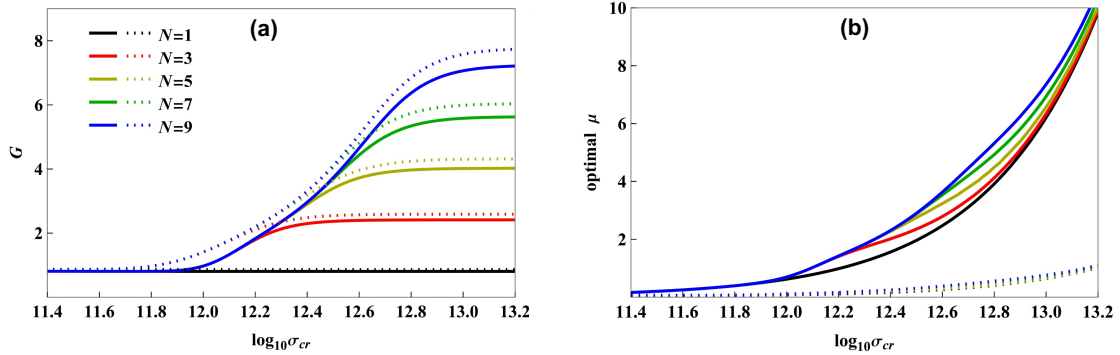


Figure 10: (a) The gain function, defined with Eq. (24), plotted against the EPMF width, σ_{cr} , for the pump laser pulse duration equal to $\tau_p = 333$ ns. The plots are maximized over the mean number of photon pairs emitted by the SPDC source in a single polarization mode, μ . Different colors of the lines correspond to various numbers of WDM channel pairs, N , utilized by Alice and Bob, as shown on the legend. The transmission profile of the WDM channels is assumed to be rectangular and their center angular frequencies are defined according to Eq. (6). The separation between the neighboring channels is equal to $\omega_{sep} = 2\pi \times 100$ GHz, while their width is taken to be either $\Delta\omega = 2\pi \times 10$ GHz (solid lines) or $\Delta\omega = 2\pi \times 10$ GHz (dotted lines). All the results are calculated for the transmittance of the channels connecting the source with the trusted parties equal to $T = 10^{-3}$. (b) The optimal values of μ , corresponding to the results illustrated in panel (a).

when the WDM channel transmission profile is Gaussian. In this case the key generation rate for $\sigma_{cr} \rightarrow \infty$ reaches values that are approximately 50% lower than for $\sigma_{cr} = 100$ GHz. This decrease coincides with the increase of the ratio between the probability for only signal photon to enter the proper WDM channel, p_{+-}^{Gaus} , and the probability for both signal and idler photons to enter the considered channel pair, p_{++}^{Gaus} , as illustrated in Fig. 11 (b). It should be mentioned here that since the considered setup configuration is symmetric, the probability for only idler photon to enter a given WDM channel pair, p_{-+}^{Gaus} is always equal to p_{+-}^{Gaus} . While the ratio $p_{+-}^{\text{Gaus}}/p_{++}^{\text{Gaus}}$ is negligible for $\sigma_{cr} = 100$ GHz, it approximately reaches the value of 0.5 for $\sigma_{cr} \rightarrow \infty$. However, the events in which only one of the SPDC photons enters a given WDM channel pair can contribute only to the random coincidences, in which case the probability for error is 50%. Thus, increasing $p_{+-}^{\text{Gaus}}/p_{++}^{\text{Gaus}}$ makes the QBER grow, lowering the obtainable key generation rate in comparison with the case of rectangular WDM channel profile, for which the ratio of $p_{+-}^{\text{rect}}/p_{++}^{\text{rect}}$ remains negligibly small for all the relevant pairs of values of σ_{cr} and τ_p .

It turns out that when the EPMF width becomes high enough for other WDM channel pairs to significantly contribute to the overall key generation rate, the ratio of $p_{+-}^{\text{Gaus}}/p_{++}^{\text{Gaus}}$ calculated for them is approximately the same as for the central channel pair. Therefore, $K_{\text{WDM}}^{\text{total}}$ that can be obtained by the trusted parties when using WDM modules with Gaussian transmission profile is about two times lower than in the case of rectangular profiles, regardless of how many channel pairs Alice and Bob use in total. For realistic WDM modules, with channel transmission profiles steeper than the Gaussian function, one should expect the gain function to take values in between the results for Gaussian and rectangular profiles presented in Fig. 11 (a).

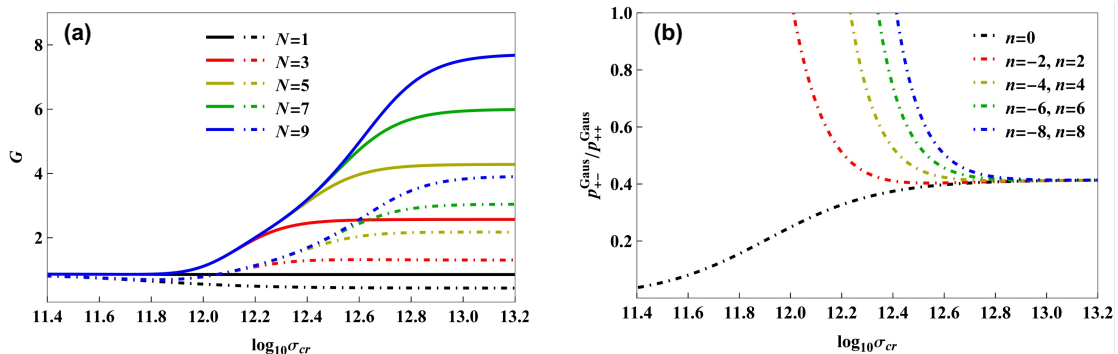


Figure 11: (a) The gain function, defined with Eq. (24), plotted against the EPMF width, σ_{cr} , for the pump laser pulse duration equal to $\tau_p = 333$ ns. The plots are maximized over the mean number of photon pairs emitted by the SPDC source in a single polarization mode, μ . Different colors of the lines correspond to various numbers of WDM channel pairs, N , utilized by Alice and Bob, as shown on the legend. The transmission profiles of WDM channels is assumed to be either rectangular, given by Eq. (4) with the width of $\Delta\omega = 2\pi \times 50$ GHz (solid lines), or Gaussian, given by Eq. (5) with the standard deviation of $\sigma_f = 2\pi \times 50$ GHz (solid lines) (dotted lines). The central angular frequencies of the WDM channel pairs utilized by the trusted parties are defined according to Eq. (6). All the results are calculated for the transmittance of the channels connecting the source with the trusted parties equal to $T = 10^{-3}$. (b) The ratio between the probability for only Alice's photon to enter the WDM channel belonging to the pair denoted by number n , p_{+-}^{Gaus} , and the probability for both photons from an SPDC pair to enter this channel pair, given by the formulas (17) and (13) respectively, plotted as a function of the EPMF width for $\tau_p = 333$ ns.

5 Summary and outlook

In this manuscript we theoretically analyzed the possibility for increasing the key generation rate produced by the QKD system, executing entanglement-based version of the BB84 protocol with the use of an SPDC source, by employing WDM modules. These devices can be utilized to split the signal and idler photons with different wavelengths into separate detection systems and perform multiple key generation processes in parallel. In order to maximize the key rate provided by such setup configuration we performed optimization of the SPDC source over the EPMF width of the utilized nonlinear crystal and the intensity and duration of the pump laser pulses. The results were compared with the key rate produced by the traditional QKD system, showing the potential for significant improvement.

We investigated both the cases of the SPDC source generating strongly negative and strongly positive spectral correlation between the signal and idler photons. For the negative correlation scenario the number of WDM channel pairs that can contribute to the overall key rate is determined primarily by the EPMF width, while the pump laser pulse duration is responsible for the key rate obtainable from individual WDM channel pairs. When the spectral correlation is positive, the correlated WDM channel pairs have to be defined in different way and the roles of the aforementioned parameters are reversed. We showed that, considering currently available technology, the optimal value of the pump laser pulse duration for the negative correlation case mainly depends on the recovery time of the utilized QKD setup elements. On the other hand the required EPMF width relies on the number of WDM channel pairs the trusted parties are willing

to employ. As an example this quantity should be at least of the order of 10 THz to enable key generation from more than ten WDM channel pairs. Meanwhile, the overall key generation rate in the positive correlation case is maximized when both the aforementioned source parameters are the smallest. In order to exploit full potential from ten WDM channel pairs in this situation the EPMF width and pump laser pulse duration should be no larger than 10 GHz and 100 fs, respectively.

The results for the overall key generation rate obtained in our analysis exhibit weak dependence over the WDM channel width. We investigated both Gaussian and rectangular transmission profile for these channels, showing approximately two times larger overall key generation rate for the latter case when the source parameters are optimized. The presented analysis was performed with several simplifying assumptions. In particular, only noiseless case was considered, with the ideal photon-number-resolving detectors used by the trusted parties. Therefore, the results are most relevant for the medium communication distance, such as can be found in typical metropolitan networks.

In the future we plan to continue this research by investigating the influence of noise on the obtained results in various configurations of the detection systems and considering the effects of chromatic dispersion in typical single-mode fibers. Furthermore, in order to build the bridge between our work and Ref. [18], where the idea of utilizing WDM modules to increase the key generation rate of the QKD system was first proposed, we intend to compare the key generation rates that can be produced with the use of pulsed and continuous-wave pump lasers.

Acknowledgements

The authors acknowledge financial support from the project ‘‘Secure quantum communication in multiplexed optical networks’’ run by the National Science Centre (NCN) in Poland as a part of the OPUS 20 + LAP programme (grant no. 2020/39/I/ST2/02922).

Appendix

Basing on the theory presented in Ref. [35] one can derive the following formula for the probability for a type-II SPDC source to generate k photon pairs in a single polarization mode in total:

$$\begin{aligned} \pi(k) &= \sum_{k_1=0}^k \sum_{k_2=0}^{k-k_1} \cdots \sum_{k_{M-1}=0}^{k-k_1-\cdots-k_{M-2}} \frac{(\mu\lambda_0)^{k_1}}{(\mu\lambda_0+1)^{k_1+1}} \frac{(\mu\lambda_1)^{k_2}}{(\mu\lambda_1+1)^{k_2+1}} \times \cdots \times \frac{(\mu\lambda_{M-2})^{k_{M-1}}}{(\mu\lambda_{M-2}+1)^{k_{M-1}+1}} \\ &\times \frac{(\mu\lambda_{M-1})^K}{(\mu\lambda_{M-1}+1)^{K+1}}, \end{aligned} \quad (28)$$

where μ is the mean number of the produced pairs, $K = \sum_{s=1}^{M-1} k_s$ and λ_m is the relative strength of the m -th mode, that can be expressed in terms of the parameters σ_{cr} and τ_p as

$$\lambda_m = \frac{8\sigma_{cr}\tau_p(2 - \sigma_{cr}\tau_p)^{2m}}{(2 + \sigma_{cr}\tau_p)^{2m+2}}. \quad (29)$$

In principle the summation in Eq. (28) should be performed over infinite number of modes. However, because $0 < \lambda_{m+1}/\lambda_m < 1$, the contribution of the modes with numbers higher than M to the probabilities $\pi(k)$ becomes negligible provided that sufficiently large value of M is taken. Unfortunately, since the EPMF widths and pump laser pulse durations relevant for our

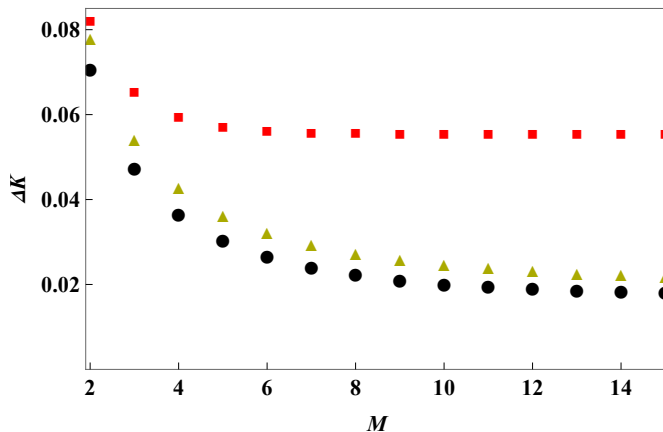


Figure 12: Relative detuning of the key generation rate caused by approximating the real statistics of photon pairs emitted by the SPDC source in a single polarization mode by the Poisson probability distribution, defined in Eq. (30), plotted as a function of the number of modes M considered in the calculation of the real statistics. Different colors and styles of the points correspond to the following values of the $\sigma_{cr}\tau_p$ product: $\sigma_{cr}\tau_p = 9.5$ (red squares), $\sigma_{cr}\tau_p = 30$ (black circles), $\sigma_{cr}\tau_p = 0.1$ (yellow triangles). The plots are made for only the single WDM channel pairs utilized by Alice and Bob ($N = 1$).

investigation are such that $\sigma_{cr}\tau_p \gg 1$ ($\sigma_{cr}\tau_p \ll 1$) for the case of strongly negative (positive) spectral correlation considered in Sec. 4.2 (Sec. 4.3), the number of modes contributing to the real photon pair statistics is large. Thus, the numerical calculations of $K_{\text{WDM}}^{\text{total}}$, needed to generate the results presented in the main body of this manuscript, could not be done effectively with the use of Eq. (28). However, in the limit of infinitely strong spectral correlation, *i.e.* when either $\sigma_{cr}\tau_p \rightarrow \infty$ or $\sigma_{cr}\tau_p \rightarrow 0$, the statistics of the produced photon pairs take the form of Poisson probability distribution [35]. Therefore, we performed all the aforementioned calculations with the probabilities $\pi(k)$ approximated by Poisson statistics.

In order to assess the impact of this approximation on the presented results let us define the relative detuning of the key generation rate

$$\Delta K(M) = \frac{K_{\text{WDM},M}^{\text{total}} - K_{\text{WDM,Poisson}}^{\text{total}}}{K_{\text{WDM,Poisson}}^{\text{total}}}, \quad (30)$$

where $K_{\text{WDM},M}^{\text{total}}$ is the overall key rate calculated when utilizing the photon pair probability distribution given by Eq. (28) with M modes involved, while $K_{\text{WDM,Poisson}}^{\text{total}}$ is the analogous result obtained with the use of Poisson probability distribution. The relative detuning of the key generation rate is an asymptotically decreasing function of M , as can be seen in Fig. 12, where it is plotted for the case of $N = 1$ and three different values of the $\sigma_{cr}\tau_p$ product. The results do not depend on the number of WDM channel pairs considered in this calculation. For $\sigma_{cr}\tau_p \approx 9.5$, which is the smallest value relevant for our analysis in the case of negative spectral correlation, $\Delta K(M) \lim_{M \rightarrow \infty} 0.055$. The value of this function drops below 0.02 for $\sigma_{cr}\tau_p = 30$. Corrections of $K_{\text{WDM}}^{\text{total}}$ of this order would be barely visible in the figures regarding negative spectral correlation case presented in the main body of this manuscript. Furthermore, the difference would become even smaller for the pairs of values of the EPMF width and the pump laser pulse duration allowing for substantial overall key rate improvement with use of the considered WDM method.

Similar verdict can be delivered in the case of positive spectral correlation, where the largest value of $\sigma_{cr}\tau_p$ relevant to our calculation is 0.1. In this situation $\Delta K(M) \lim_{M \rightarrow \infty} 0.021$, as can be also seen in Fig. 12. Therefore, the assumed Poisson approximation of the statistics of photon pairs emitted by the SPDC source does not influence any of the conclusions drawn in this manuscript.

References

- [1] S. Pirandola, U. L. Andersen, L. Banchi, M. Berta, D. Bunandar, R. Colbeck, D. Englund, T. Gehring, C. Lupo, C. Ottaviani, J. L. Pereira, M. Razavi, J. Shamsul Shaari, M. Tomamichel, V. C. Usenko, G. Vallone, P. Villoresi, and P. Wallden. Advances in quantum cryptography. *Adv. Opt. Photon.*, 12:1012–1236, 2020.
- [2] G. Brassard, N. Lütkenhaus, T. Mor, and B. C. Sanders. Limitations on practical quantum cryptography. *Phys. Rev. Lett.*, 85:1330–1333, 2000.
- [3] L. Zhou, J. Lin, Y.-M. Xie, Y.-S. Lu, Y. Jing, H.-L. Yin, and Z. Yuan. Experimental quantum communication overcomes the rate-loss limit without global phase tracking. *Phys. Rev. Lett.*, 130:250801, 2023.
- [4] Y. Liu, W.-J. Zhang, C. Jiang, J.-P. Chen, C. Zhang, W.-X. Pan, D. Ma, H. Dong, J.-M. Xiong, C.-J. Zhang, H. Li, R.-C. Wang, J. Wu, T.-Y. Chen, L. You, X.-B. Wang, Q. Zhang, and J.-W. Pan. Experimental twin-field quantum key distribution over 1000 km fiber distance. *Phys. Rev. Lett.*, 130:210801, 2023.
- [5] Y. Zhang, Z. Chen, S. Pirandola, X. Wang, C. Zhou, B. Chu, Y. Zhao, B. Xu, S. Yu, and H. Guo. Long-distance continuous-variable quantum key distribution over 202.81 km of fiber. *Phys. Rev. Lett.*, 125:010502, 2020.
- [6] M. Lasota, O. Kovalenko, and V. C. Usenko. Robustness of entanglement-based discrete- and continuous-variable quantum key distribution against channel noise. *New J. Phys.*, 2023.
- [7] W. H. Louisell, A. Yariv, and A. E. Siegman. Quantum fluctuations and noise in parametric processes. i. *Phys. Rev.*, 124:1646–1654, 1961.
- [8] D. C. Burnham and D. L. Weinberg. Observation of simultaneity in parametric production of optical photon pairs. *Phys. Rev. Lett.*, 25:84–87, 1970.
- [9] E. Pomarico, B. Sanguinetti, T. Guerreiro, R. Thew, and H. Zbinden. Mhz rate and efficient synchronous heralding of single photons at telecom wavelengths. *Opt. Express*, 20:23846–23855, 2012.
- [10] S. Ramelow, A. Mech, M. Giustina, S. Gröblacher, W. Wieczorek, J. Beyer, A. Lita, B. Calkins, T. Gerrits, S. W. Nam, A. Zeilinger, and R. Ursin. Highly efficient heralding of entangled single photons. *Opt. Express*, 21:6707–6717, 2013.
- [11] F. Kaneda, K. Garay-Palmett, A. B. U’Ren, and P. G. Kwiat. Heralded single-photon source utilizing highly nondegenerate, spectrally factorable spontaneous parametric downconversion. *Opt. Express*, 24:10733–10747, 2016.

- [12] S. Fasel, O. Alibart, S. Tanzilli, P. Baldi, A. Beveratos, N. Gisin, and H. Zbinden. High-quality asynchronous heralded single photon source at telecom wavelength. *New J. Phys.*, 6:163, 2004.
- [13] M. Bock, A. Lenhard, C. Chunnillall, and C. Becher. Highly efficient heralded single-photon source for telecom wavelengths based on a ppln waveguide. *Opt. Express*, 24:23992–24001, 2016.
- [14] P. Kok and S. L. Braunstein. Postselected versus nonpostselected quantum teleportation using parametric down-conversion. *Phys. Rev. A*, 61:042304, 2000.
- [15] W. Helwig, W. Mauerer, and C. Silberhorn. Multimode states in decoy-based quantum-key-distribution protocols. *Phys. Rev. A*, 80:052326, 2009.
- [16] K. Sedziak, M. Lasota, and P. Kolenderski. Reducing detection noise of a photon pair in a dispersive medium by controlling its spectral entanglement. *Optica*, 4:84–89, 2017.
- [17] M. Lasota and P. Kolenderski. Optimal photon pairs for quantum communication protocols. *Sci. Rep.*, 10:20810, 2020.
- [18] J. Pseiner, L. Achatz, L. Bulla, M. Bohmann, and R. Ursin. Experimental wavelength-multiplexed entanglement-based quantum cryptography. *Quantum Sci. Technol.*, 6:035013, 2021.
- [19] G. P. Agrawal. *Fiber-Optic Communications Systems*. John Wiley & Sons, Inc., New York, NY, 2002.
- [20] P. D. Townsend. Simultaneous quantum cryptographic key distribution and conventional data transmission over installed fibre using wavelength-division multiplexing. *Electron. Lett.*, 33:188–190, 1997.
- [21] P. Eraerds, N. Walenta, M. Legré, N. Gisin, and H. Zbinden. Quantum key distribution and 1 gbps data encryption over a single fibre. *New J. Phys.*, 12:063027, 2010.
- [22] B. Qi, W. Zhu, L. Qian, and H.-K. Lo. Feasibility of quantum key distribution through a dense wavelength division multiplexing network. *New J. Phys.*, 12:103042, 2010.
- [23] P. D. Townsend. Quantum cryptography on multiuser optical fibre networks. *Nature*, 385:47–49, 1997.
- [24] W. Sun, L.-J. Wang, X.-X. Sun, Y. Mao, H.-L. Yin, B.-X. Wang, T.-Y. Chen, and J.-W. Pan. Experimental integration of quantum key distribution and gigabit-capable passive optical network. *J. Appl. Phys.*, 123:043105, 2018.
- [25] J. F. Dynes, A. Wonfor, W. W.-S. Tam, A. W. Sharpe, R. Takahashi, M. Lucamarini, A. Plews, Z. L. Yuan, A. R. Dixon, J. Cho, Y. Tanizawa, J.-P. Elbers, H. Greißer, I. H. White, R. V. Pentyl, and A. J. Shields. Cambridge quantum network. *NPJ Quantum Inf.*, 5:101, 2019.
- [26] C. H. Bennett and G. Brassard. Quantum cryptography: Public key distribution and coin tossing. In *Proceedings of the IEEE International Conference on Computers, Systems, and Signal Processing, Bangalore, India*, volume 11, pages 175–179. IEEE, New York, 1984.

- [27] T. Lutz, P. Kolenderski, and T. Jennewein. Demonstration of spectral correlation control in a source of polarization entangled photon pairs at telecom wavelength. *Opt. Lett.*, 39:1481–1484, 2014.
- [28] A. Gajewski and P. Kolenderski. Spectral correlation control in down-converted photon pairs. *Phys. Rev. A*, 94:013838, 2016.
- [29] K. Sedziak-Kacprowicz, M. Lasota, and P. Kolenderski. Remote temporal wavepacket narrowing. *Sci. Rep.*, 9:3111, 2019.
- [30] G. E. Keiser. A review of wdm technology and applications. *Opt. Fiber Technol.*, 5:3–39, 1999.
- [31] V. Scarani, H. Bechmann-Pasquinucci, N. Cerf, M. Dušek, N. Lütkenhaus, and M. Peev. The security of practical quantum key distribution. *Rev. Mod. Phys.*, 81:1301–1350, 2009.
- [32] N. Lütkenhaus. Quantum key distribution: theory for application. *Appl. Phys. B*, 69:395–400, 1999.
- [33] B. Kraus, N. Gisin, and R. Renner. Lower and upper bounds on the secret-key rate for quantum key distribution protocols using one-way classical communication. *Phys. Rev. Lett.*, 95:080501, 2005.
- [34] R. Renner, N. Gisin, and B. Kraus. Information-theoretic security proof for quantum-key-distribution protocols. *Phys. Rev. A*, 72:012332, 2005.
- [35] W. Maurer, M. Avenhaus, W. Helwig, and C. Silberhorn. How colors influence numbers: Photon statistics of parametric down-conversion. *Phys. Rev. A*, 80:053815, 2009.